AD

AD-E404 067

Technical Report ARMET-TR-17073

DEVELOPMENT OF A METHOD FOR MODELING THE RESPONSE OF A LIQUID-FILLED DEFORMABLE PIPE TO AN IMPACT LOAD

Catherine S. Florio

September 2018

U.S. ARMY ARMAMENT RESEARCH, DEVELOPMENT AND ENGINEERING CENTER

Munitions Engineering Technology Center

Picatinny Arsenal, New Jersey

REPORT DOCUMENTATION PAGE

Form Approved
OMB No. 0704-01-0188

1. REPORT DATE (DD-MM-YYYY)	2. REPORT TYPE	3. DATES COVERED (*From - To*)
September 2018	Final	February 2017 to April 2017

4. TITLE AND SUBTITLE

DEVELOPMENT OF A METHOD FOR MODELING THE RESPONSE OF A LIQUID-FILLED DEFORMABLE PIPE TO AN IMPACT LOAD

5a. CONTRACT NUMBER

5b. GRANT NUMBER

5c. PROGRAM ELEMENT NUMBER

6. AUTHORS

Catherine S. Florio

5d. PROJECT NUMBER

5e. TASK NUMBER

5f. WORK UNIT NUMBER

7. PERFORMING ORGANIZATION NAME(S) AND ADDRESS(ES)
U.S. Army ARDEC, METC
Armaments Engineering Analysis & Manufacturing Directorate (RDAR-MEA-A)
Picatinny Arsenal, NJ 07806-5000

8. PERFORMING ORGANIZATION REPORT NUMBER

9. SPONSORING/MONITORING AGENCY NAME(S) AND ADDRESS(ES)
U.S. Army ARDEC, ESIC
Knowledge Management Office (RDAR-EIK)
Picatinny Arsenal, NJ 07806-5000

10. SPONSOR/MONITOR'S ACRONYM(S)

11. SPONSOR/MONITOR'S REPORT NUMBER(S)
Technical Report ARMET-TR-17073

12. DISTRIBUTION/AVAILABILITY STATEMENT

Approved for public release; distribution is unlimited.

13. SUPPLEMENTARY NOTES

14. ABSTRACT

A comparison of methods is presented to model the effect of an impact-based pressure wave in a fluid medium on the behavior of a deformable pipe with one closed end that contains the fluid. The predicted pipe deformation and fluid pressures using Lagrangian elements, Eulerian elements, continuum particle elements, and acoustic elements are evaluated, and the benefits and limitations of the use of each element type to model this system are discussed. Based on these comparisons, a method using acoustic elements and an acoustic medium material model to represent the nonflowing fluid in this system is presented, which shows good correlation in predicted transient fluid pressure and pipe wall deformation to experimental measurements.

15. SUBJECT TERMS

Impact load Pressure wave propagation Element type Acoustic elements Deformable pipe

16. SECURITY CLASSIFICATION OF:			17. LIMITATION OF ABSTRACT	18. NUMBER OF PAGES	19a. NAME OF RESPONSIBLE PERSON
a. REPORT	b. ABSTRACT	c. THIS PAGE			Catherine Florio
U	U	U	SAR	33	19b. TELEPHONE NUMBER (Include area code) (973) 724-8267

Standard Form 298 (Rev. 8/98)
Prescribed by ANSI Std. Z39.18

CONTENTS

	Page
Introduction	1
Methods	2
System Studied	2
Material Properties	2
Boundary and Initial Conditions	3
Method Development	4
Output Measures Considered	11
Results	11
Lagrangian Elements	12
Eulerian Elements	16
Continuum Particle Elements	19
Acoustic Elements	20
Discussion	22
Selected Method	22
Model Limitations	23
Conclusions	24
References	25
Distribution List	27

FIGURES

1	System studied	2
2	Input pressure curve	4
3	Geometric representations	6
4	Pressure variation with time normal to the fluid surface at the closed end of the small diameter region of the pipe system studied	12
5	Axial stress in system	13
6	Piston diameter is less than pipe diameter (note: deflection scaled 1x)	14
7	Typical results with Eulerian elements	17
8	Typical results with Eulerian elements when the with different initial volume ratios	18
9	Typical results with continuum particle elements	19

FIGURES
(continued)

Page

10 Typical results with acoustic elements 21

11 Use of model with acoustic elements to predict dynamic pipe burst behavior 23

ACKNOWLEDGMENTS

This work was funded by the Institute for Special Warfare at the U.S. Army Armament Research, Development and Engineering Center, Picatinny Arsenal, NJ. Adam Foltz provided the experimental data and images.

INTRODUCTION

The propagation of pressure waves through a fluid that completely fills a pipe structure induces dynamic forces against the pipe wall that deform the wall and impose resultant forces back on the system fluid, altering the local fluid pressures as the wall deforms. As a result, the local interactions affect both the pipe structure and the wave characteristics of the input pressure. The ability to model this interaction allows for the detailed study of both media and can improve the understanding of the effects of system variations in geometry, material properties, and boundary conditions. From the reduction of the adverse effects of the water hammer phenomena that develops upon sudden valve closure to the design of pipe structures that withstand explosive-based shock inputs, such a model could contribute to the improved understanding and design of such mixed fluid-structure systems. This development of a computational modeling method to study such a system is the focus of the current work.

Analytical models of the interaction between a deformable tube and an internally contained fluid have been the subject of much study for applications from structural pipes and blood vessels (refs. 1 to 3). However, the solutions are typically limited by the assumptions required to find these analytical solutions. Such simplifying assumptions typically restrict the tube geometry, wall thickness, and material properties, the fluid flow regime, compressibility, and fluid properties, and the dimensionality of the pressure wave propagation, reflection, and interaction.

Computational methods offer the study of a wider range of systems and conditions than most analytical models of these fluid-structure systems. More complex geometry and pipe materials can be examined (ref. 4). More complex flow conditions can be explored, and time-dependent thermal changes in the fluid or solid component can easily be included (ref. 5). Most importantly, through such a computational tool, variations to these parameters can readily be studied without a significant reformulation of the model used to evaluate the system. For these reasons, an efficient computational model method was developed in this work that can be implemented to study the effect of the propagation of a pressure wave through a nonflowing fluid that completely fills a deformable pipe structure.

While modeling the interaction of fluid and solid media can be accomplished in a number of ways, each has unique challenges, especially under short durations typical of pressure wave propagations. Three main methods include (1) using a computational fluid dynamics code and adjusting element formulations and/or material properties to represent the deformable solid behavior, (2) using a finite element code and making similar adjustments to represent the behavior of the fluid, and (3) directly coupling the two types of code so each solves for the behavior of a single medium and passes information back and forth as boundary conditions. The use of coupled codes can provide detailed predictions of the phenomena that occur in both media. However, there is a significant computational cost with this method. In addition, compatibility issues can arise in the use of output data from one software as input for another software. The use of a single code may allow for an efficient prediction of a desired behavior of interest under an appropriate set of modeling assumptions. The selection of either a fluids-based or structural-based code can be made based on which phenomena is of most interest. If the influence of the deformable structure on the fluid behavior, especially for a flowing, viscous fluid, is the focus of the study, the inclusion of a fluids-based code may be more suitable. However, in this study, the behavior of the structure is of most interest, and the fluid is nonflowing and nearly incompressible. Therefore, finite element based methods are the focus of this work.

METHODS

In this study, a method to efficiently model the propagation of an impact pressure wave through a fluid contained within a deformable pipe and predict the resulting behavior of the pipe was developed. The general method development and an application will be described. Because the pressure wave is responsible for the local deformations in the pipe, both an accurate prediction of the propagation of the pressure wave through the fluid and the transfer of the energy to the pipe were of interest.

System Studied

The developed method is intended to be used on an arbitrary fluid-filled pipe system. A specific geometry is presented here with which the function of the developed method was evaluated. The selected system contains a number of loading modes on both the pipe and the fluid so that the capabilities of the developed method may be evaluated. However, the method can be applied to any system of a deformable pipe structure filled with a nonflowing fluid.

In this particular study, a water-filled, stepped-diameter pipe with one closed end was examined. An impact load was imparted to the free surface of the water on the open end of the pipe via a piston rod. The pipe was held within a fixture that restricted its motion as a result of the impact load (fig. 1). The central region of the larger diameter region of the pipe was unconstrained. Only the pipe behavior in this unconstrained region was of interest. The two segments of the pipe were the same length, and the ratio of the larger to smaller inner diameters of the pipe was 3.3. The pipe had a wall thickness that was about one-seventh of the larger inner diameter of the pipe.

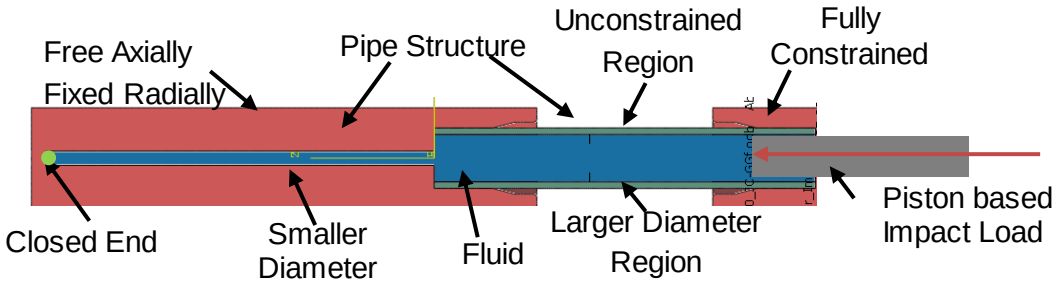

Note: Green point indicates of pressure measurement.

Figure 1
System studied

Material Properties

The system consisted of three materials: the pipe, the fixture, and the fluid. The system was evaluated at ambient thermal conditions. As with the geometry, the materials can be arbitrarily selected. For the representative case studied here, the specific material properties are presented. The fixture was made of stainless steel T600 (ref. 6). The fluid was water (ref. 7). The pipe was made of an electronic-resistance-weld seamed tube of standard black pipe steel (ref. 8). Based on the pipe standard ASME B31 [developed by the American Society of Mechanical Engineers (ref. 9)], the reduction factor of the allowable pipe pressure due to this kind of weld is 15%. Therefore, the material strength was reduced in a region of the pipe that represented the weld by this amount. This region ran down the length of the large diameter region of the pipe and through the pipe wall thickness. The weld region width was two mesh elements wide.

While the behavior of the fixture steel was assumed to be linearly-elastic (table 1), the strain-dependent plastic behavior of the pipe was incorporated in this model. Specifically, a Johnson-Cook

plastic stress model (eq. 1a) was used. Based on the pressure load input curve (see Boundary and Initial Conditions section), the strain rate effect during the short duration increase to the constant pressure impact pulse is negligible and was ignored in this material model. A Johnson-Cook damage initiation model (eq. 1b) with damage evolution was used in the weld region only. Parameters were based on those of steel with similar carbon content and adjusted as necessary to represent the yield strength of schedule 40 black pipe (refs. 10 and 11).

Table 1
Material properties of fixture and pipe

Component	Material	Density (lbf-s^2/in.^4)	Elastic modulus (x10^6) psi	Poisson's ratio
Fixture	Stainless steel T600	7.332e-4	29.0	0.29
Pipe	Schedule 40 black pipe (steel)	7.332e-4	29.5	0.29

$$\sigma = [A_1 + A_2\varepsilon^N][1 + A_3 ln\dot{\varepsilon}]$$

$$\sigma = 60000 + 39900\varepsilon^{0.36} \quad (1a)$$

$$\varepsilon_f = \left[D_1 + D_2 e^{C\frac{\sigma_p}{\sigma_{VM}}}\right]\left[1 + D_3 ln\frac{\dot{\varepsilon}}{\dot{\varepsilon}_0}\right]$$

$$\varepsilon_f = \left[2.07e^{1.22\frac{\sigma_p}{\sigma_{VM}}}\right] \quad (1b)$$

Where A_i , D_i,, *C, and N* are empirically derived constants, ε_f is the failure strain, σ_P is the dilatational pressure stress, and σ_{VM} is the von Mises stress.

The water material behavior was described by its bulk modulus and density. The bulk modulus of water at room temperature and atmospheric pressure, 320 ksi, was used in this model. Similarly, the density of water at room temperature and atmospheric pressure, 9.35815e-5 lbf-s^2/in^4, was assumed in this work. The water was represented as a static, constant mass system incompressible fluid.

The speed of sound in a medium is defined as C_0

$$C_0 = \sqrt{\frac{K}{\rho_0}} \quad (2)$$

For water, as described previously, C_0 is 59,221 in./s.

Boundary and Initial Conditions

The fixture held the pipe constrained in all degrees of freedom at the plunger end. On the opposite end of the unconstrained larger diameter region of the pipe and throughout the length of the smaller diameter region, the pipe was prevented from net radial or rotational displacement about the axis. Axial displacement was permitted on this end of the pipe, allowing the pipe to stretch or compress axially in response to the transient fluid pressure. The pipe was closed on the end opposite that of the piston such that no fluid flow occurred in the system.

The piston imparted an axially-directed impact load to the free surface of the water filling the pipe. While this impact could be used to produce an arbitrary load and time-history, a near-step

impact pressure load was selected for this study. The duration time of this impact event was selected to be longer than the time needed for the pressure wave to travel down the pipe and back so that no shock occurred. The step curve describing the impact load to the free surface of the water had a short linear transition to and from atmospheric pressure at the beginning and end of the time studied. A typical curve is shown in figure 2. These physical transition regions also prevented the numerical instabilities that would result in the computational model if a true mathematical step function was used as the input pressure load.

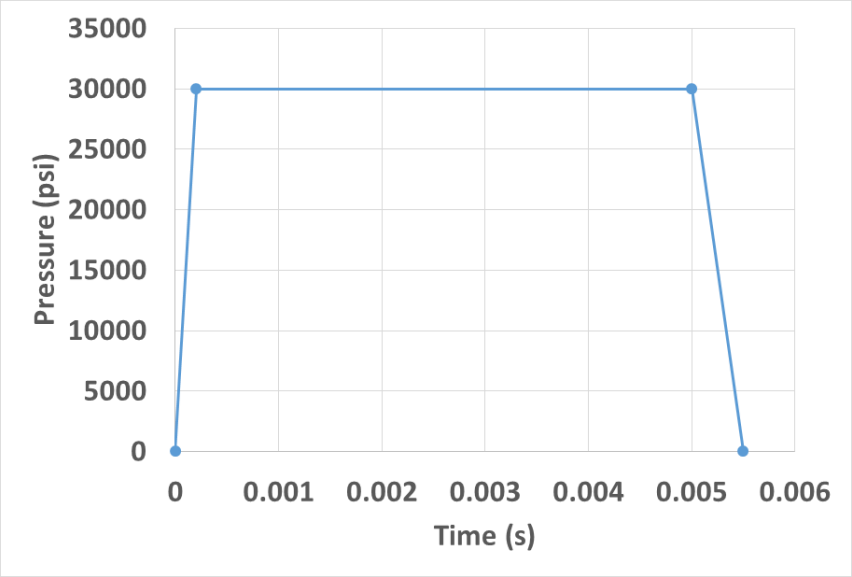

Figure 2
Input pressure curve

During and after the impact event, the water was required to maintain contact with all of the solid surfaces to which it was initially in contact. The impact event was designed such that the speed of the pressure wave was less than that of the speed of sound in water. Because no shock event occurred, no discontinuities along the wave front existed, and this phenomenon did not need to be considered in the computational model.

Method Development

The development of an efficient method to predict the behavior of the unconstrained region of the pipe in the system of figure 1 was the intent of this work. Because the behavior of the structural component of the system was the main interest, a finite element based method was used. However, because the pressures in the fluid created the boundary conditions of the pipe region of interest, an accurate prediction of the pressure wave propagation through the fluid was required. To study this fluid behavior using a finite element based method, the main concern is related to the means with which to represent the conditions in the fluid. This was the focus of the current study. The commercial finite element software Abaqus was used for this study (ref. 12).

A number of methods to model the fluid in this system were investigated. Specifically, the fluid was represented by Lagrangian elements, Eulerian elements, continuum particle elements, and acoustic elements. Each method is presented so that the strengths and weaknesses for the application of interest can be compared. Based on the evaluation of each of these modeling methods, the one that best represented both the pressure wave propagation and the response of the pipe in the system depicted in figure 1 was selected. The evaluation of the candidate methods was based on comparisons of the time-dependent pressure at the closed end of the pipe system to

experimentally-collected data for the representative case studied. To ensure proper prediction of the pipe behavior, qualitative comparisons were made between timing and extent of deformation in the pipe predicted by the modeling method developed and those captured via high-speed video under experimental condition. As this behavior is also affected by the material model and properties used to represent the pipe, the focus was on the location of maximum deformation and initial failure, which are more directly dependent on the fluid local fluid pressures. For all methods, the pipe, fixture, and plunger were represented by Lagrangian elements with an explicit formulation. The impact event examined was studied using a transient dynamic analysis.

Both axisymmetric and three-dimensional (3-D) models were analyzed in this preliminary study (fig. 3). In each case, linear hexahedral elements were used in all regions. The comparison of the different representations of the fluid was performed on a simplified geometry that did not initially contain the welded region of pipe so that an axisymmetric or one-quarter symmetry model could be used. Comparisons focused on differences in measured pressure from experimentally measured results. The model that best predicted this pressure was then used in a full 3-D geometry with the welded seam to examine the ability to predict the failure behavior of the pipe. While the models may have varied slightly in the details of the geometry of the pipe and fixtures, the dimensions that defined the stress, displacement, and fluid pressure behavior were consistent through all cases studied.

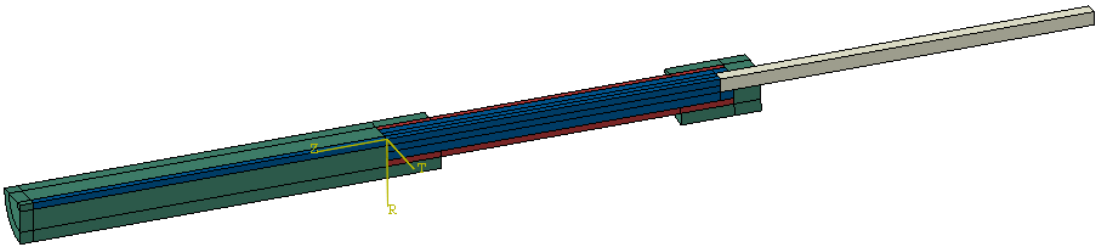

(a)
3-D quarter symmetry with plunger

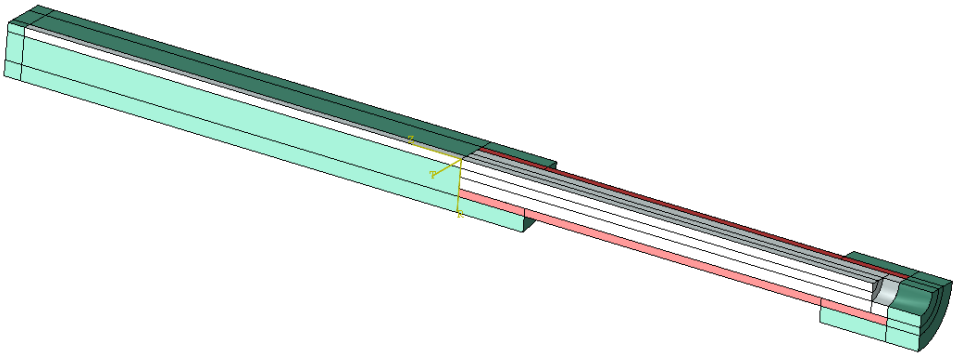

(b)
3-D quarter symmetry without piston

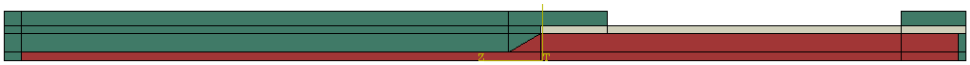

(c)
Axisymmetric with pusher plate representing piston

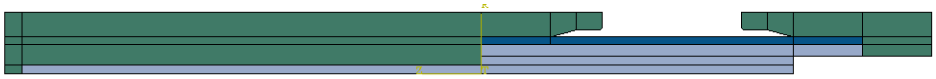

(d)
Axisymmetric without piston

Figure 3
Geometric representations

Lagrangian Elements to Represent the Fluid

The simplest means of representing the nonflowing, constant mass volume of fluid in the studied system using a finite element based modeling method is with Lagrangian elements. These elements are the standard continuum elements used in a structural finite element code. In their typical formulation, they can calculate stresses and deformations within parts and transfer energy from one component to the next through contacting interfaces. In this element formulation, the force and displacement are coupled through the implementation of a modified form of the momentum equation that is based on virtual work. Elements have displacement-based degrees of freedom, and stresses are calculated based on the deformation of these elements. Both dilatational and deviatoric stresses are considered, and neither one may be directly excluded. When

deformation is large, the Lagrangian analysis can be coupled with mesh adaptation methods to maintain the mesh integrity under the studied loads (refs. 13 and 14).

For this study using Lagrangian elements, the water material was represented by a solid (i.e., not porous), homogenous, and elastic material. The elastic modulus was set to be the bulk modulus of water at room temperature and atmospheric pressure, 312 ksi. As the fluid (water) is considered nearly incompressible, a Poisson's ratio of 0.45 was used. The density of water at room temperature and atmospheric pressure, 8.896e-5 lbf-s^2/in^4, was also used.

Because the fluid exhibits a no-slip boundary condition at the interfaces with the solid components of the system, contact parameters were applied to prevent separation at the interface between the water and the pipe and between the water and the plunger. A number of modeling methods to achieve this behavior were studied. One involved a tie constraint between the surfaces of the water and the mating surfaces in the pipe and plunger. Other methods included using a "rough" friction formulation in the tangential direction, which prevents slip once contact is achieved. This "rough" frictional formulation was coupled with a no separation normal behavior. This was examined with and without the inclusion of a cohesive interface behavior. The cohesive behavior was applied to exert the default traction-separation behavior on any slave node experiencing contact. For the purposes of the model, the water was the slave surface since it responded to the impact imparted by the plunger.

The model was also evaluated with and without a physical representation of the plunger rod. With no plunger rod, a pressure was used as a boundary load on the free surface of the fluid (fig. 3b). With either representation, the applied pressure had a tendency to deform the elements near this loaded surface. However, the no-slip condition prevented these elements from moving from the surface. This can result in potentially large deformation of the individual elements near the solid surfaces. Therefore, a number of adaptive remeshing parameters were examined. For remeshing to be used in Abaqus, the region that is being remeshed and all regions in contact with it must be comprised of tetrahedral, triangular, or quadrilateral-dominated meshes that were made by the advancing front method (ref. 15). With this modification, different frequencies of remeshing (ranging from every timestep to every five timesteps), number of sweeps at each remeshing event (ranging from 1 to 5), initial feature angle to be used to identify elements to remesh (ranging from 0 to 180 deg), and constraint angles identifying the target desired element angles after remeshing (ranging from 80 to 100 deg), and momentum advection types that control the local extent and distribution of remeshing effects through the remeshing region (half index shift and element center projection) were tried. The half index shift momentum advection has better dispersion properties than the element center projection and is recommended for cases of wave propagation (ref. 15). As most of the problematic element deformation occurred along the interfaces, initially perpendicular element faces should be maintained after remeshing. Therefore, the chosen range of constraint angles varied around 90 deg. These modeling features were used in various combinations to examine the potential use of the Lagrangian element formulation to represent the liquid in the system in figure 1 for the conditions of interest in this study.

Eulerian Elements to Represent the Fluid

With the Eulerian element formulation, the elements have no displacement degrees of freedom. Elements do not deform. Instead, the material flows from one element to the next (ref. 13). The initial level of fill of each element is specified, and the analysis proceeds by passing the mass from one element to the next in response to the applied conditions (refs 13 and 14). Because the water is nearly incompressible, the initial fill of each element was varied from 50 to 99.5% of the element volume. No inflow was allowed at any surface of the water. This includes the free surface where the load was applied. The same surface interactions and inclusion/exclusion of the plunger geometry were examined with the Eulerian elements. Due to the formulation of Eulerian-Lagrangian

interfaces, which is based on an immersed boundary method, if the Lagrangian body is initially positioned outside the Eulerian mesh, one layer of void Eulerian elements is required at the boundary so that Eulerian material driven out of the interior elements has a place to go (ref. 16). Because the Eulerian elements do not deform, no adaptive meshing was needed.

In some of the cases, the effect of using an equation of state material model for the fluid was also examined. The equation of state material model ignores the deviatoric behavior of the material and assumes that pressure is a function of volume changes only. For the nonflowing, constant mass fluid system studied in this work, such conditions represented in the equation of state material model were thought to improve the prediction of the propagation of the pressure wave through the fluid over that of a standard model intended for solid deformable materials.

With the energy equation, the equation of state directly couples pressure to energy. The energy equation can be written in the following form such that the pressure is separated into its components due to the dilatational and deviatoric stresses (ref. 17). With no heat generation, the energy equation becomes:

$$\rho \frac{\partial E_m}{\partial t} = (P - P_{bv}) \frac{1}{\rho} \frac{\partial \rho}{\partial t} + \mathbf{S} : \dot{\mathbf{e}} \tag{4}$$

Where ρ is the current material density, E_m is the energy per unit mass, P is the dilatational pressure stress (positive in compression), P_{bv} is the dilatational pressure stress due to the bulk viscosity, $\mathbf{S}$ is the deviatoric stress tensor, and $\dot{\mathbf{e}}$ is the deviatoric part of the strain rate (ref. 17).

The equation of state is unique to a particular material and describes the current pressure as a function of the current density ρ and the internal energy per unit mass E_m (ref. 17). The internal energy in equation 3 can be decoupled from the relation describing the current pressure so that the pressure is described solely as a function of density. This form of the pressure is called the Hugoniot pressure $P_H = f(\rho)$ (ref. 17). This is determined experimentally. Similarly, the Hugoniot pressure can be defined only as a function of density E_H such that (ref. 17):

$$E_H = \frac{\left(1 - \rho_0/\rho\right) P_H}{2\rho_0} \tag{5}$$

Where ρ_0 is the initial material density. The term $1 - \rho_0/\rho$ is given the symbol η and represents the nominal volumetric compressive strain (ref. 17).

A Mie-Gruneisen equation of state with a linear (Us-Up) Hugoniot form was used. In this model, the equation of state is a linear function of energy (ref. 17):

$$P - P_H = \Gamma \rho (E_m - E_H) \tag{6}$$

Where Γ is a particular function of the material and is defined as (ref. 17):

$$\Gamma = \Gamma_0 \rho_0/\rho \tag{7}$$

Combining equations 5 through 7, the Mie-Gruneisen equation of state could be written as (ref. 17):

$$\mathrm{P} = P_H \left(1 - \frac{\eta \Gamma_0}{2}\right) + \Gamma_0 \rho_0 E_M \tag{8}$$

The pressure-density relationship in the Hugoniot equation can be represented by a relation with two material-specific parameters (ref. 17):

$$P_H = \frac{\rho_0 \eta c_0^2}{(1-s\eta)^2} \tag{9}$$

The two material-specific parameters c_0 and s further relate the shock and particle velocities (ref. 17).

$$U_S = c_0 + sU_p \tag{10}$$

Where U_S is the shock velocity, U_p is the particle velocity, c_0 is the speed of sound in the medium at atmospheric pressure, and s is a proportionality constant that depends on the material. Note that c_0 and ρ are further related as they describe the elastic bulk modulus, K, of the material through the relation in equation 2 (ref. 17).

In the conditions examined in this study, the shock velocity is constant and equal to the speed of sound in the fluid (water). s is set to zero. Thus (ref. 17):

$$U_S = c_0 \tag{11}$$

Further, the pressure in the water is assumed to be only a function of volume changes only, having no deviatoric component. Thus, Γ_0 is set to zero, and (ref. 17):

$$\mathrm{P} = P_H = f(\rho) \tag{12}$$

Through these assumptions and forms, the equation of state material model can be used to represent a material that has no stresses generated due to shearing, which corresponds to the conditions in the volume of water filling the pipe under the impact load.

Continuum Particle Elements to Represent the Fluid

The use of continuum particle elements in a smoothed particle hydrodynamics (SPH) formulation to represent this system of interest was also examined. It was thought that this "meshless" formulation may help enforce the no-slip interface conditions as it would eliminate the issue of element deformation. In this formulation, the solution at a particular particle is a weighted sum of that of a set of surrounding particles. The weighting factor is a function of distance from the particular particle. It is important to note that the solution becomes less accurate than Lagrangian for small deformations and less accurate than coupled Eulerian-Lagrangian analyses for very large deformations. However, when the material void ratio is very small, Eulerian analyses may be very computationally intensive, and SPH may be more efficient (refs. 13 and 16).

The SPH solution is known to have accuracy issues near boundaries with Lagrangian elements that can propagate through the whole SPH region (ref. 16). As a result, a method has been developed and is implemented in the commercial code used in this study (Abaqus) where a virtual plane is created and ghost particles are created to simulate a free slip or no-slip boundary surface behavior (ref. 16). The particle solution in the SPH field are then computed based on the solution of the ghost particles (ref. 16). In this analysis, the no-slip boundary surface behavior was implemented.

For simplicity, the SPH discretization was automatically generated by the commercial finite element code through a conversion from a conventional finite element mesh that was created through standard meshing techniques. One particle per node was used, but various element sizes

were examined. Cubic weighting function was used to describe the influence of neighboring particles. Both the default, classical SPH method and the normalized SPH method were used to calculate the updated location of the particles (refs. 13 and 16).

Acoustic Elements to Represent the Fluid

Finally, the use of an acoustic element formulations and an acoustic medium material model to represent the fluid was evaluated. This type of element formulation and the corresponding material model are useful in examining the propagation of a wave, including a shockwave, through a medium. Acoustic elements can also interact with structural elements to simulate transfer of between the deformable solid and the acoustic medium. This can be used to evaluate the effect of a wave on a structure and also the development of a wave due to the motion of a structure. Acoustic elements can also be used to study emission and radiation phenomenon and can be used to predict cavitation in a fluid (ref. 13). Acoustic elements do not physically deform, as they have a single degree of freedom, which is pressure (refs. 13 and 14). As such, shear stresses must be assumed to be negligible in the system studied (refs. 13 and 14). Therefore, like the equation of state formulation used with the Eulerian elements, stresses are assumed to be dilatational only, and strain is only volumetric. Because of these characteristics, the use of acoustic elements and an acoustic medium material model were thought to comply with the modeling intent of this study.

The acoustic medium is assumed to be inviscid, linear, adiabatic, and compressible, and the fluid flow and mass transfer are assumed to be negligible (ref 18). The pressure is described as a function of the bulk modulus and the velocity at each point in the medium (ref 1).

$$\mathrm{P} = -K_f(\mathbf{x},\theta_i)\frac{\partial}{\partial \mathbf{x}} \cdot \mathbf{u} \tag{13}$$

Where K_f, the bulk modulus, can vary with location within the medium $\mathbf{x}$ and field properties θ_i of the water like temperature, humidity, or chemical composition. $\mathbf{u}$ is the local velocity of the displacement of the fluid.

The momentum equation is then reduced to (ref. 18):

$$\frac{\partial P}{\partial \mathbf{x}} + \gamma(\mathbf{x},\theta_i)\dot{\mathbf{u}} + \rho(\mathbf{x},\theta_i)\ddot{\mathbf{u}} = 0 \tag{14}$$

Velocity-dependent momentum losses are represented with a "volumetric drag" $\gamma(\mathbf{x},\theta_i)$, which has units of force per unit volume per velocity (refs. 17 and 18).

The acoustic medium interacts with the boundaries through various impedances. Boundaries can be fully reflective, fully absorptive/transmissive, fully radiative, or a combination of any of these in varying degrees (ref. 19). If the behavior of only the acoustic medium is of interest, impedance effects of the solid can be simulated with these impedance boundary conditions. If the behavior of response of the solid to the acoustic medium is of interest, the two element types can be coupled through their normal displacements (ref. 16 and 19). The normal displacements can be further dissipated to represent some damping at the interfaces such as would occur in a porous structure or soft layer (ref. 18). The tangential displacements remain uncoupled (refs. 18 and 19).

Because the momentum is transferred between the acoustic medium and the solid or between two different acoustic media through nodal displacements, the relative element size becomes important. The mesh refinement depends on the wave speeds of the two media. In general, the medium with the lower wave speed should have the more refined mesh (ref. 19). If the wave behavior at the interface is important, the two media should have similar element sizes that correspond to the level of refinement of the slower wave speed (ref. 19). The code developer

recommends that the mesh is set such that at least six nodes per wavelength of the medium are available (ref. 19) where:

$$\lambda f = c \tag{15}$$

λ is the wavelength, the wave frequency is f, and the wave speed is c, which can be calculated for the material as in equation 2. In this study, the wavelength was 296 in., and the element size used was approximately 0.025 in.

The input load for an acoustic element is a pressure acting on an internal or external surface because its only degree of freedom is pressure. The pressure can only act normal to the surface (refs. 16 and 19). Alternatively, the pressure can propagate from a point source (ref. 16). This is common in a shock or blast analysis. If the effects of a shockwave are of interest, additional material models are needed to handle the discontinuities that develop at the shock front. Such effects are not included in this work, and the additional material models are, therefore, not presented here. It should be noted that the input pressure load must be dynamic when using the built in acoustic elements in Abaqus, representing the change in the pressure as a result of the wave studied. An additional, initial static pressure can be pre-assigned. Otherwise, it is assumed that the system is initially at atmospheric conditions (ref. 17).

In the current model, the initial static pressure was assumed to be atmospheric. The plunger was not modeled directly but was represented by a pressure load at the free surface normal to the pipe axis. As in the other models studied, the plunger diameter was smaller than the pipe diameter. The sides of the plunger, therefore, were represented by purely reflective impedances at these boundaries of the acoustic medium representing the water. All walls of the pipe were considered to be fully reflective and coupled with the fluid through surface-to-surface tied constraints. Because the influence of the pressure within the acoustic medium on the structural response of the pipe was of interest, the acoustic medium was selected to be the master of the contact pairs with each solid surface. The acoustic medium material properties consisted simply of the density of the water and the bulk modulus, defined previously. The pressure load was arbitrarily selected and was the same that was applied in each of the other studies (fig. 2).

Output Measures Considered

Each of these models was used to simulate the system and condition of interest for the same impact load (fig. 2). The pressure measured at the end of the smaller diameter pipe was tracked for each case (shown as the green dot in fig. 1). Because this pressure was also measured in an experimental representation of the system studied, it was used as the basis of comparison among the models examined in this study. In addition, qualitative observations of the behavior of the deformable pipe were compared to provide a better understanding of the effects of each of the element types studied. Finally, run time and ease of convergence were considered. From this evaluation of the four methods of representing the fluid in this system, the most appropriate method for modeling the conditions of interest was selected.

RESULTS

Each of the four models examined resulted in unique behaviors that are directly related to the element formulations and their limitations. The applicability of each to the system examined in this work is presented in the following paragraphs.

Lagrangian Elements

With the Lagrangian solid continuum elements, the propagation of the stress wave through the pipe material and the resulting deformation was well defined. The stresses in the large diameter section of the pipe varied with the pressures that developed in the fluid in this region of the system. However, the propagation of the water "pressures" into the small diameter region of pipe did not seem to be properly captured. With an impact pressure of 30,000 psi, the maximum pressure at the closed end of the smaller diameter region only reached 2,500 psi and oscillated about 0 psi (fig. 4). Additionally, the direction of the axial displacement of the pusher plate began to oscillate with time as the fluid material, represented by an elastic solid, compressed and locally deformed the pipe. This locally expanded the pipe. The amount of displacement of the plunger was greater than the volume change due to the radial expansion of the deformable pipe. As the water material was further compressed, elastic energy was stored in the material. With time, the stored energy became sufficient to overcome the applied pressure from the piston. This forced the piston in a direction opposing the impact load and resulted in the oscillations seen (fig. 5).

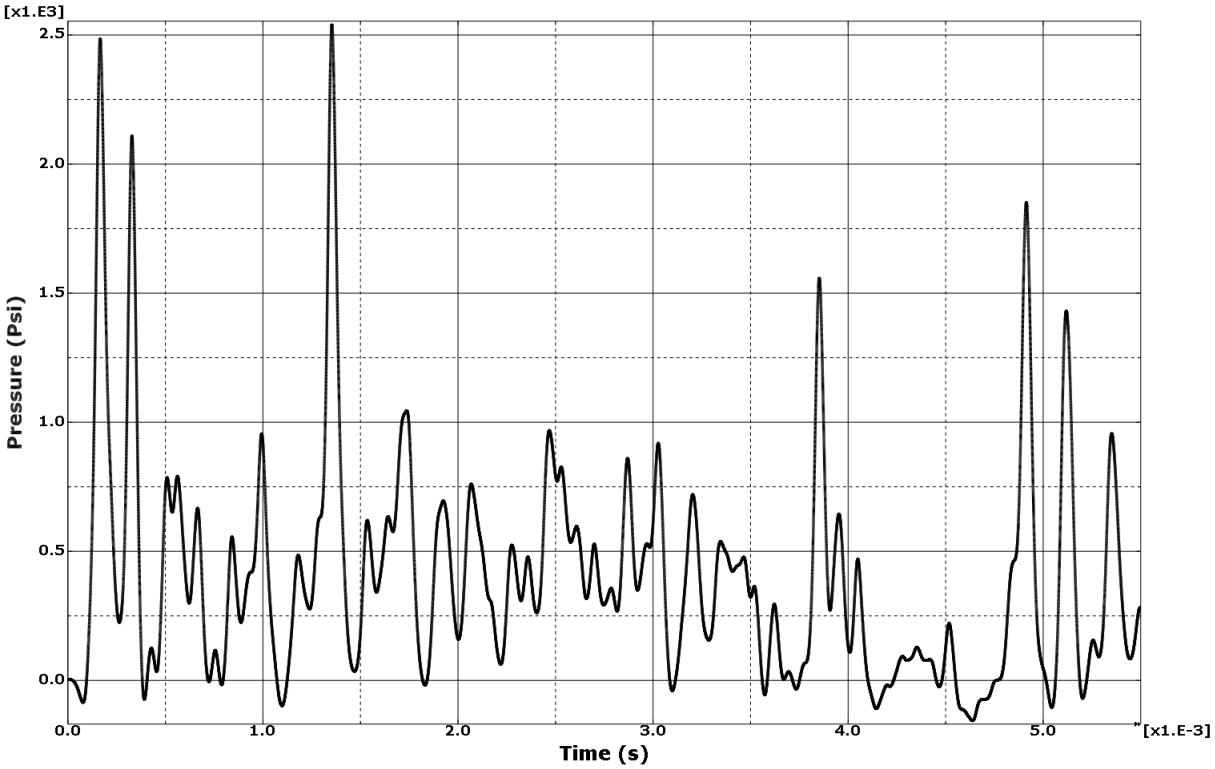

Figure 4
Pressure variation with time normal to the fluid surface at the closed end of the small diameter region of the pipe system studied

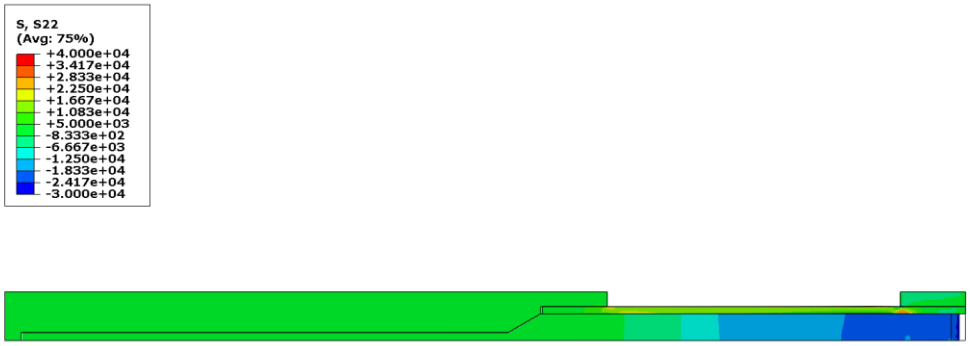

(a)
Approximately 0.05 ms (startup)

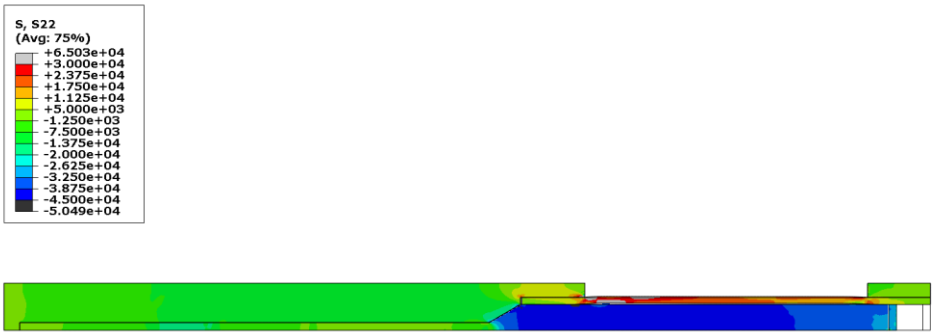

(b)
Approximately 0.2 ms (maximum applied pressure)

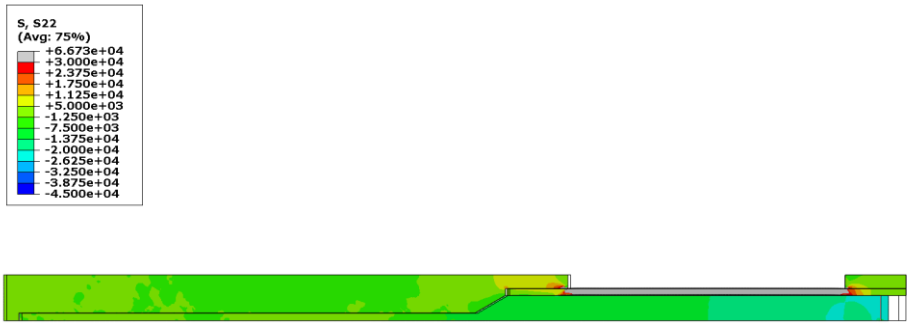

(c)
Approximately 0.4 ms (region of constant applied pressure)

Note: Deflection scaled 1x, and original configuration noted by wireframe.

Figure 5
Axial stress in system

When the diameter of the piston was reduced to less than the inner diameter of the wider section of the pipe, the effects of the element deformation from the deviatoric stresses calculated in these Lagrangian elements were more notable. Various mesh adaptation parameters and interaction models were examined as described previously. None, however, were sufficient to

alleviate the large deformation at the edge of the piston that results from the elastic material model and the required no-slip boundary condition between the fluid and the pipe (fig. 6). This combination of allowing elastic deformation of the fluid volume but requiring it to maintain contact at all times with all solid surfaces lead to the element distortion issues seen using the Lagrangian elements with an elastic material model to represent the fluid. This was further complicated by the limitation in Abaqus/Explicit code that the no separation contact restriction can only be used with a rough contact formulation. This is very similar to the use of a tied interface, and it requires nodes in initial contact to remain in contact. If this restriction was relaxed, the water would separate from the rear wall of the fixture when it becomes sufficiently compressed by the impact load of the piston. This separation, while likely with solid volumes, is not typically feasible with the fluid studied in this system.

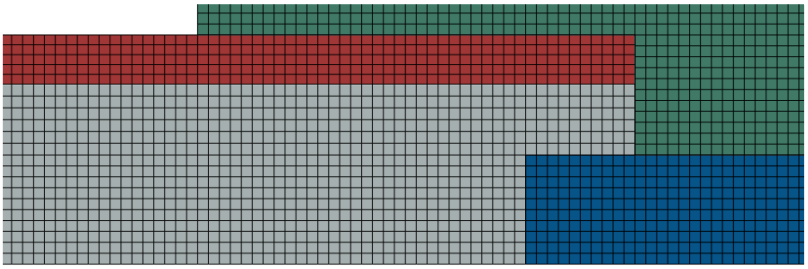

(a)
Initial mesh

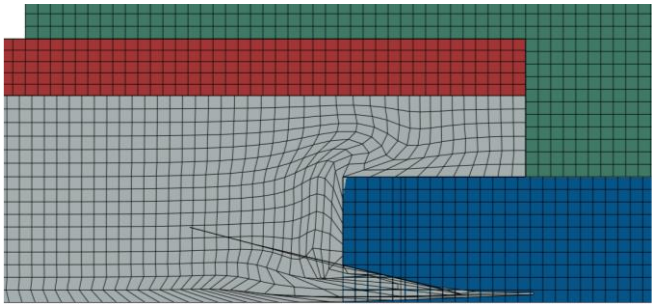

(b)
No adaptive meshing

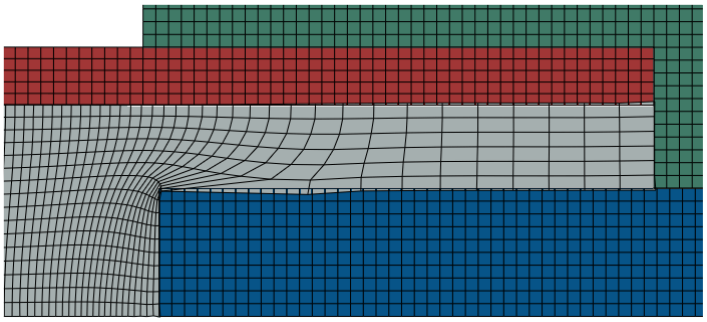

(c)
All default settings and five adaption sweeps

Figure 6
Piston diameter is less than pipe diameter (note: deflection scaled 1x)

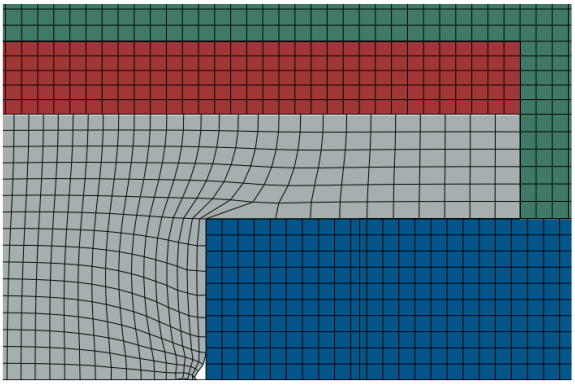

(d)
All default adaption parameters, every five timesteps, five adaption sweeps

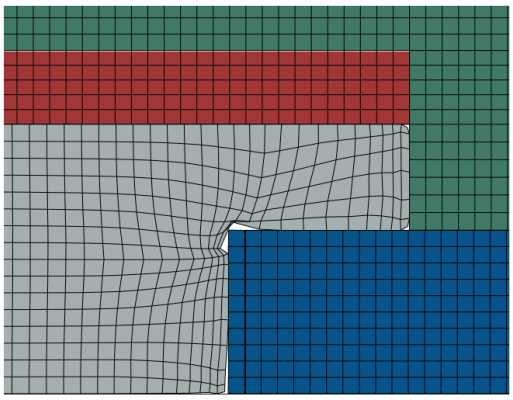

(e)
Same as in (d) and initial angle 180 deg, constraint angle 85 deg, transition feature angle 60 deg, half index shift momentum advection

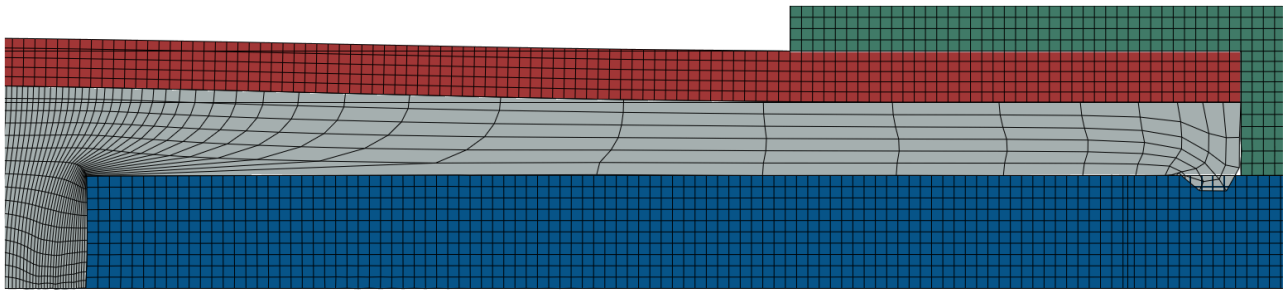

(f)
Same as in (d) constraint angle 85 deg, transition feature angle 0 deg, half index shift momentum advection

Figure 6
(continued)

This model-predicted behavior that results from using Lagrangian elements and a homogeneous elastic material model to represent the fluid does not appear to follow what would be expected of the physical behavior of a non-Newtonian, nearly incompressible, nonflowing fluid.

Therefore, this modeling method is not likely to produce an appropriate representation of the system of interest.

Eulerian Elements

The Eulerian elements with an equation of state material model did not have the deformation and mesh distortion problems that occurred with the Lagrangian elements with the homogenous elastic material model. Additionally, the pressure wave propagation was better predicted than was with the Lagrangian elements, as the graduated increase of "pressure" stresses along the axial length of the pipe was clearly visible in the water, and larger stresses were seen in the small diameter region of the pipe than in the larger diameter region (fig. 7a). However, no analysis proceeded past the "startup" portion of the pressure curve. By 0.2 ms, the time step was reduced a number of orders of magnitude from that at the start of the analysis. This occurred because of very high pressures that developed in the corners near the closed end of the pipe and near the plunger (fig. 7b). Pressures in this region were two orders of magnitude greater than in the rest of the water volume. Changing the Eulerian outflow type, the initial impact pressure, and the mesh did not alleviate this problem. This occurred with and without a physical representation of the piston.

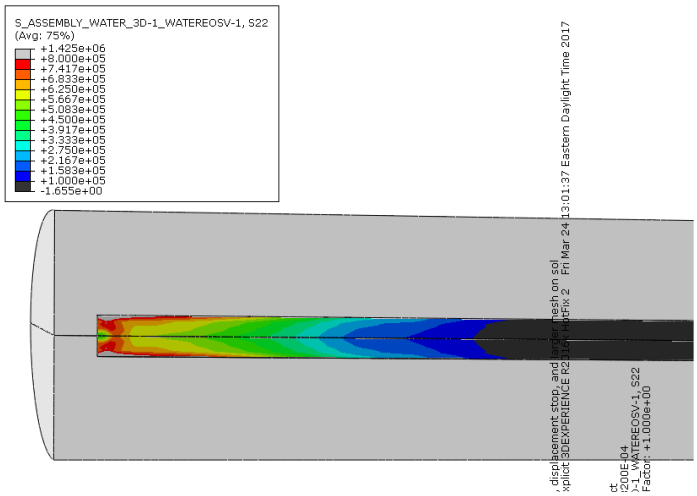

(a)
Region of high stress

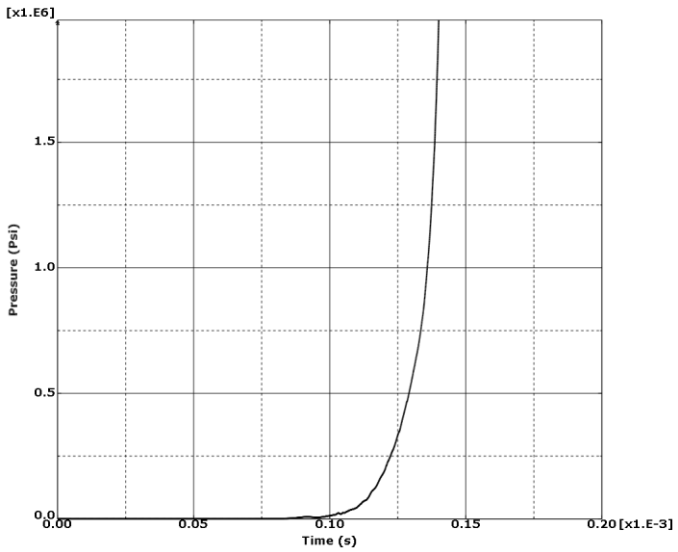

(b)
Maximum stress in this region with time

Figure 7
Typical results with Eulerian elements

Further, when a no-slip interface was enforced between the piston elements and the water elements, extreme deformation would occur in the piston (fig. 8a). This occurred because the driving momentum would cause a tendency of motion of the piston, but the interface constraint caused a tendency of no motion as there is no deformation in Eulerian elements. With the elements “nearly filled” initially, there is no room for the mass flow, which represents deformation in the Eulerian formulation. Therefore, the water acts almost like a rigid body against which the plunger is impacted. If the initial fill volume was reduced in an attempt to assist the propagation of the pressure wave, the piston moved excessively as the fluid volume is not the meshed volume but is the sum of the fill ratios of each element defining the water region (fig. 8b). Balancing this initial ratio with the desired

plunger motion or volume change due to the pipe deformation to generate the desired behavior limits the predictive ability of the model.

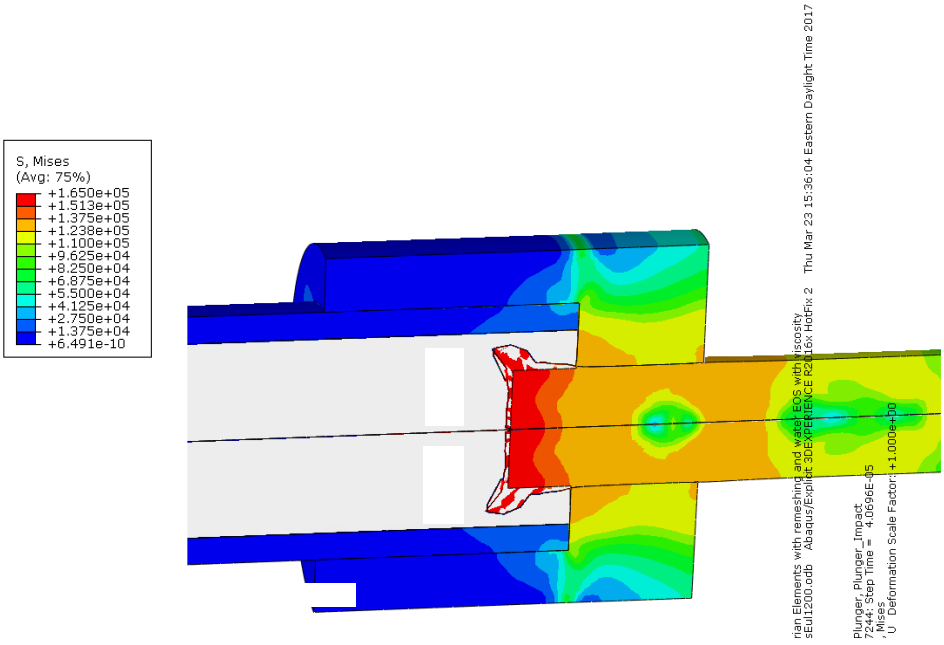

(a)
Initial volume ratio = 99.5% (nearly completely full)

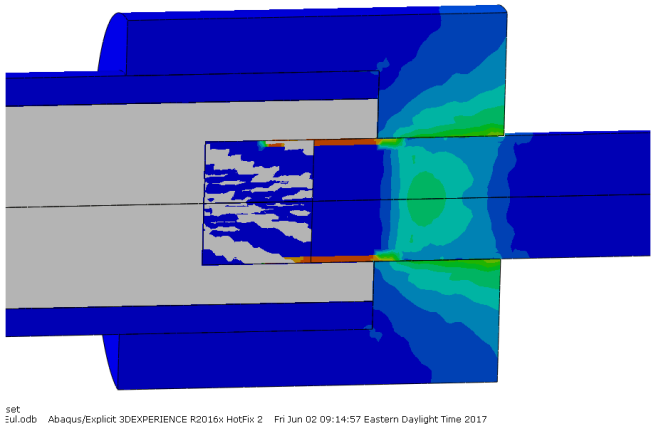

(b)
Initial volume ratio = 50% (half full)

Figure 8
Typical results with Eulerian elements when the with different initial volume ratios

Eulerian elements are intended for conditions that induce large deformations. In this model, the fluid should not significantly change its volume or shape due to the applied impact load. Therefore, the deviation from the intended use of the Eulerian element formulation in this study may have resulted in the difficulties encountered.

Continuum Particle Elements

Like Eulerian elements, continuum particle elements do not present problems with mesh distortion. Unlike Eulerian elements, however, the continuum particles do move relative to one another. Yet, because they are used with a meshless SPH solution formulation, there is no mesh to distort, which occurred when using Lagrangian elements. Unlike Eulerian elements, the full volume of the water fluid represented in the solid model is used in the solution. Therefore, the behavior of the studied system predicted by using continuum particle elements to represent the water was next examined. Because the continuum particle elements are used with a meshless SPH formulation, the entire set of particles in the volume of water examined had to be included in all interface definitions and symmetry boundary conditions. Nonetheless, difficulties arose with containing the particles within the one-quarter symmetry model. The symmetry boundary condition was violated as the simulation progressed and the displacement of the piston became excessive (fig. 9a).

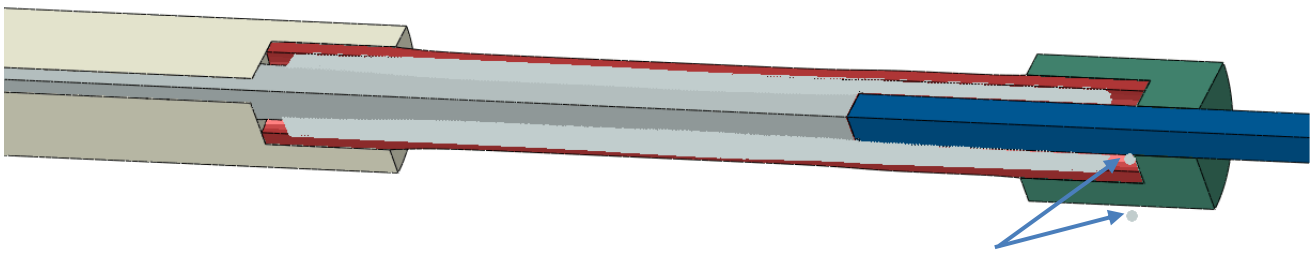

(a)
One-quarter symmetry

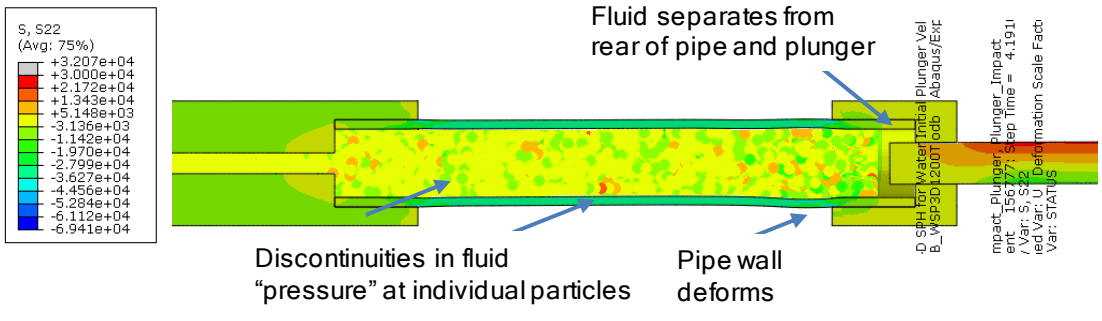

(b)
Full geometry

Figure 9
Typical results with continuum particle elements

When a full, 3-D model was used, the particles stayed within the volume, yet the movement of the piston was excessive. The deformation and stress patterns were similar to that seen with the Lagrangian element model. The "water" region separated from the back end of the pipe and, at later times, pushed the piston backward as the energy stored in the compressed medium increased. In addition, the stress distributions were not continuous, there were isolated particles of high or low magnitude stress compared to the neighboring particles, and the pressure wave did not seem to propagate down the smaller diameter region of the pipe. Deformation of the pipe wall due to the impact of the fluid was seen (fig. 9b).

As with the Eulerian elements, the continuum particle elements and the SPH method are intended to be used to study systems with large deformation. Because the system studied was incompressible, the use of these elements resulted in excessive deformation under the impact load imparted by the piston. Like the Lagrangian elements, the continuum particle elements represent a homogenous elastic medium. Therefore, they did not produce behavior like that of a fluid in the volume compressed under the impact load and separated from the solid surfaces. These disparities between the required behavior of the system studied and that produced by these three types of elements contributed to the difficulties that resulted in their use to study the current system.

Acoustic Elements

Unlike Lagrangian elements and continuum particle elements, acoustic elements do not deform under applied loads. Unlike Eulerian elements, they do not require the elements to be partially filled with the material studied. Therefore, this last element type examined to represent the fluid in the system studied was thought to mitigate the issues that were presented with each of the previous models described. The single degree of freedom of the acoustic elements, pressure, and the ability to couple the momentum and energy transfers with solid continuum elements make the system of interest potentially a good application for the use of acoustic elements with an acoustic medium material property. Therefore, the use of acoustic elements and an acoustic medium was next investigated.

With the acoustic elements, the pressure wave propagation was visible up and down both the large and small diameter regions of the pipe (fig. 10a). Additionally, the areas of large deformation in the pipe seemed to coincide with the location of high pressure in the fluid. Moreover, the split of the pressure wave is clearly visible as some is reflected on the step transition of the pipe diameter and some is propagated to the smaller diameter region (fig. 10b). The pressure at the closed end of the smaller diameter region oscillated around 20 ksi for the entire duration of the step input pressure application of 30 ksi (fig.10c). The difference between the input pressure and pressure measured at the closed end of the system is due to the losses that occur from the expansion of the pipe and the dissipation that results from the wave interactions. These three output measures predicted by the model that represented the water as an acoustic medium using acoustic elements had none of the issues seen when the water was represented with Lagrangian, Eulerian, or continuum particle elements. Therefore, this model seems the most appropriate to simulate the system and conditions of interest in this work.

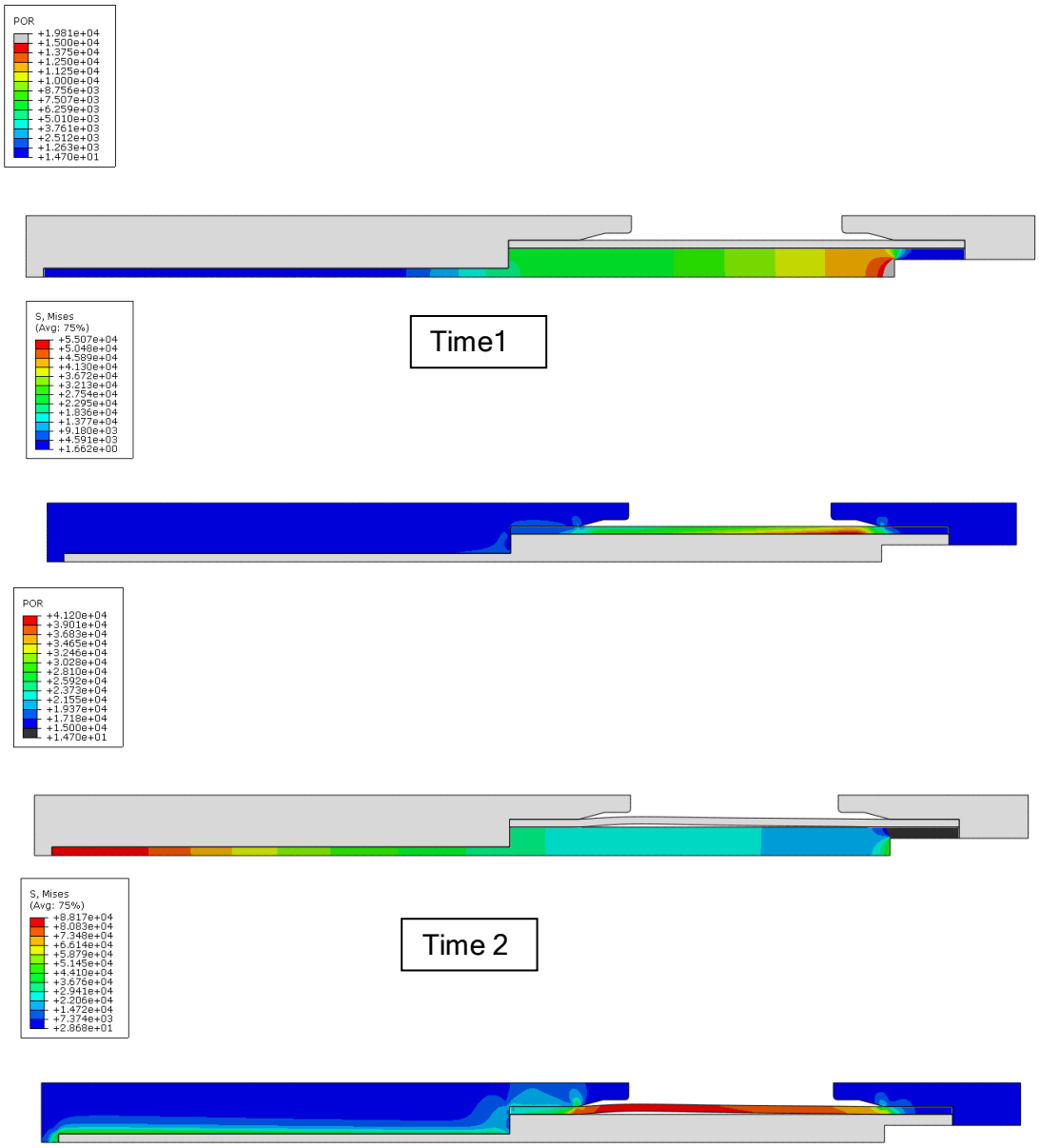

(a)
Variation in water pressure and pipe stress with time

Figure 10
Typical results with acoustic elements

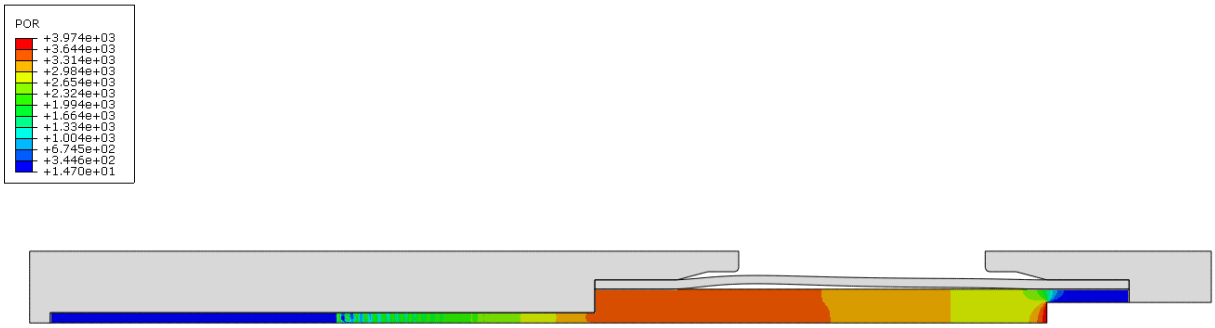

(b)
Wave behavior at step in pipe diameter

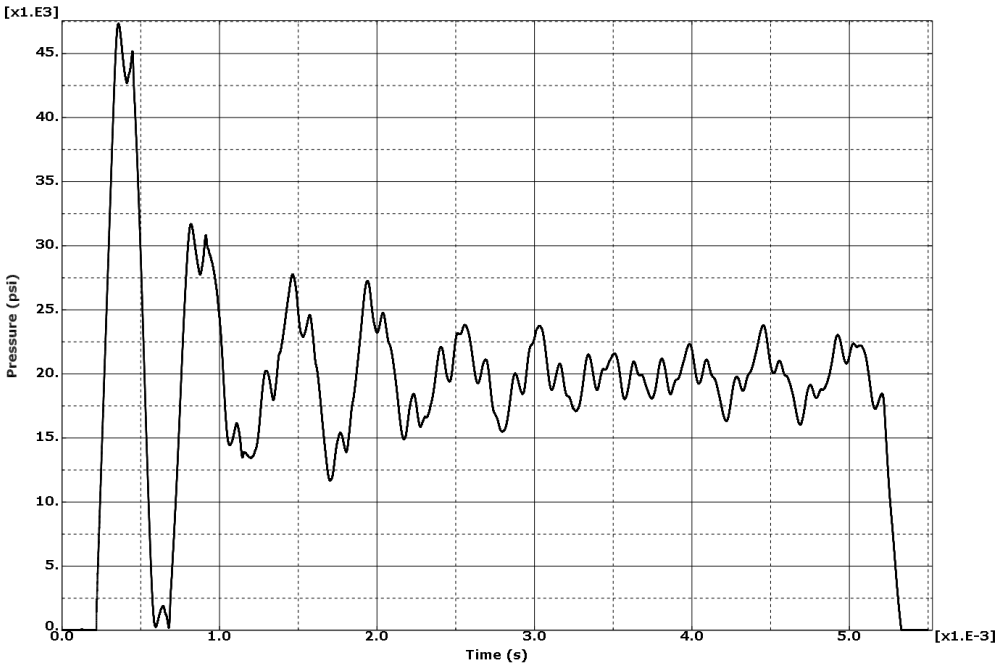

(c)
Pressure measured at closed end

Figure 10
(continued)

DISCUSSION

Selected Method

Because the acoustic elements were found to best represent the conditions studied, a full 3-D model of the pipe system and fluid was examined with this modeling method. Model results showed good quantitative prediction to experimental pressure measurements and qualitative prediction to experimentally observed failure in the pipe (ref. 20) (fig. 11). The measured pressure had the greatest variation upon initial contact with the surface representing the gage. This difference may be due to features of the physical gage that remove these large pressure variations upon initial exposure to the pressure load. This may also be related to differences in the material properties and

boundary constraints imparted on the system in the model from those of the experiment. Failure of the pipe was seen experimentally after notable expansion in the region near the downstream fixture (closer to the step change in the pipe diameter than to the impact load surface). Once the expansion was sufficient, a crack formed along the axial length of the pipe, starting from the location of greatest radial expansion. This behavior was also predicted by the model, where the failure initiated in and followed the region of weaker material properties that was meant to represent the welded seam of the pipe.

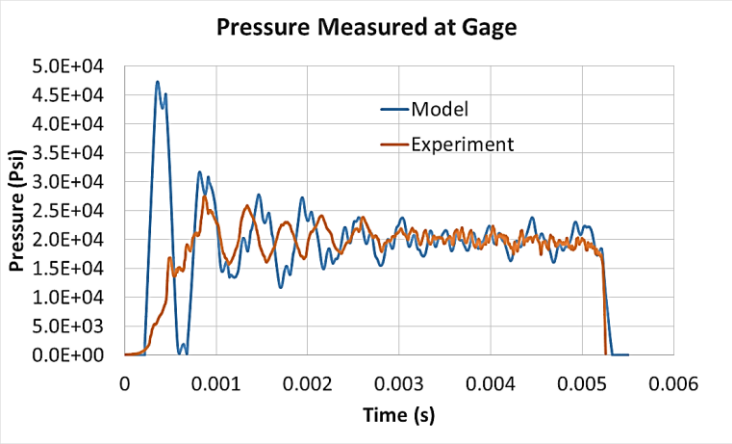

Note: Experimental data provided by A. Foltz per reference 20.

(a)
Correlation of pressure measurement at closed end of stepped pipe

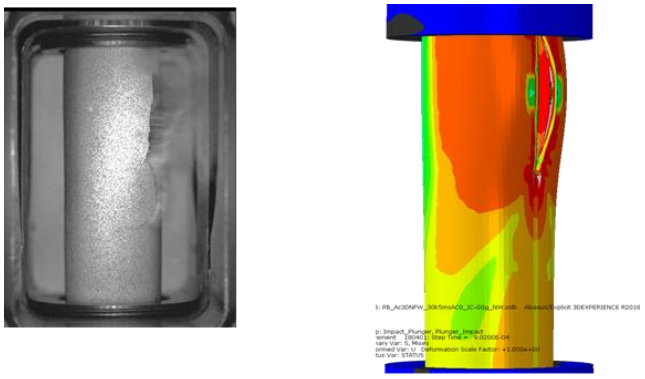

Note: Experimental data provided by A. Foltz per reference 20.

(b)
Failure of pipe at seam (left - experimental, right - computational)

Figure 11
Use of model with acoustic elements to predict dynamic pipe burst behavior

Model Limitations

The model that was selected for this system can only be used for a specific set of conditions. If the water was flowing in the pipe, shear stresses were more significant, or the volume of water changed with the impact load, Eulerian or continuum particle elements may become a more appropriate representation of the water. Because acoustic elements assume adiabatic conditions, if there was a thermal source or sink, the acoustic model could not be used to represent the fluid in this

system even with all other conditions the same, and alternative methods would be needed. Such methods would likely require coupled computational fluid mechanics to address the heat transfer phenomena and finite element methods to address the structural response.

The structural response of the pipe depends not only on the proper depiction of the fluid pressure variations but also is affected by the material properties of the fluid and solid and boundary conditions used. Strain and strain rate dependent properties of the solid are needed to capture the dynamic strains that result from the studied impact. In addition, a fully reflective impedance likely does not occur at the interfaces of the fluid and solid, as some energy must be dissipated at the interfaces. However, because the solids examined are relatively rigid, the relative amount of energy dissipated as compared to that reflected back into the fluid system is likely small, and the approximation used in this study is valid.

The smooth opening in the failed region is a result of the use of element deletion rather than a crack propagation model to represent the material failure. The inclusion of a crack propagation model may result in a more random pattern at the failed interface, which may provide a better visual comparison to experimentally tested samples. This would likely result in an increased computational cost.

CONCLUSIONS

The use of acoustic elements and an acoustic medium material to represent the nonflowing fluid filling a deformable pipe with one closed end appears to be an efficient method to simulate the propagation of an impact load applied to its free surface through the fluid and the resulting response of the deformable pipe. The presented method allows for the prediction of the propagation of a pressure wave through the medium and the transfer of energy to neighboring solid components. Because the only degree of freedom in an acoustic element is pressure, the issues associated with element distortion do not exist. These conditions provide a good representation of a nonflowing volume of fluid such as that in this study. The wave propagation and reflection at boundary surfaces, the dissipation due to the energy used to deform the surrounding surfaces, and the deformation patterns in the pipe wall are appropriately simulated. Because the elements used to model the volume of water do not deform, tracking of the change in contact status between interfacing nodes/elements is no longer necessary, reducing the overall computational resources required for the solution of the transfer of energy at the interface between the fluid and solid media. Additionally, among the types of element formulations examined in this study, good correlation between fluid pressures and failure behavior predicted by the model and those observed experimentally was found only with the use of the acoustic elements. While the specific conditions for which acoustic elements may be used are limited, for applicable systems and conditions such as the nonflowing fluid-filled pipe examined in this work, these benefits of the developed modeling technique allow the presented method to be easily implemented into parametric studies involving the effects of impact load characteristics and material properties of the solid and fluid components on the system behavior.

REFERENCES

1. Morgan, G.W. and Kiely, J.P., "Wave propagation in a viscous liquid contained in a flexible tube," Journal *of the Acoustical Society of America,* 26: 323, 1954.

2. Ando, Y., Kondo, S., Suzuoki, A., Minato, A., Tagishi, A., Nakagawa, Y., Matsushima, H., Mochizuki, K., and Mochio, T., "Experiment and analysis on pressure pulse propagation in a plastically deforming pipe," *Nuclear Engineering and Design,* 55(2):249-259, 1979.

3. Di Nucci, C. and Russo S.A., "On the propagation of one-dimensional acoustic waves in liquids," *Meccanica,* 48:15-21, 2013.

4. Mirzaei, M., Najafi, M., and Niasari H., "Experimental and numerical analysis of dynamic rupture of steel pipes under internally high-speed moving pressures," *International Journal of Impact Engineering,* 85: 27-36, 2015.

5. Hao, P.P., Pai, F., and Ma, H., "Nonlinear thermomechanical finite element modeling, analysis, and characterization of multi-turn oscillating heat pipes," *International Journal of Heat and Mass Transfer,* 69: 424-437, 2014.

6. "Stainless Steel T600," MSC Material Center Database, Accessed March 17, 2017.

7. Fox, R., McDonald, A., and Pritchard, P., "*Introduction to Fluid Mechanics*," New York, NY: Wiley and Sons, 1996.

8. ASTM International, "A53/A53M-12: Standard Specification for Pipe, Steel, Black and Hot-Dipped, Zinc-Coated, Welded and Seamless," West Conshohocken, PA, 2012.

9. The American Society of Mechanical Engineers, "ASME B31.5-2016 Refrigeration Piping and Heat Transfer Components: ASME Code for Pressure Piping B31," New York, NY, 2016.

10. Gardenier, H.E., "An Experimental Technique for Developing Intermediate Strain Rates in Ductile Metals," Master's Thesis, Air Force Institute of Technology, Wright-Patterson Air Force Base, OH, 2008.

11. Johnson, G.R., Chocron, S., Anderson, Jr, C.E., Beissel, S.R., and Holmquist, T.J., "Effect of the third invariant on strength and failure for ten metals," 27th International Symposium on Ballistics, 2012.

12. Dassault Systemes, Abaqus version 6.16-1, New Providence, RI, 2016.

13. Dassault Systemes, "Abaqus 2016 Analysis User's Guide Volume VI: Elements," New Providence, RI, 2016.

14. Dassault Systemes, "Abaqus 2016 Theory Guide Chapter 3: Elements," New Providence, RI, 2016.

15. Dassault Systemes, "Abaqus 2016 User's Guide Chapter 17: The Mesh Module," New Providence, RI, 2016.

16. Dassault Systemes, "Abaqus 2016 Analysis User's Guide Volume IV: Analysis Techniques," New Providence, RI, 2016.

REFERENCES
(continued)

17. Dassault Systemes, “Abaqus 2016 Analysis User’s Guide Volume V: Materials,” New Providence, RI, 2016.

18. Dassault Systemes, “Abaqus 2016 Theory Guide Chapter 2: Procedures,” New Providence, RI, 2016.

19. Dassault Systemes, “Abaqus 2016 Analysis User’s Guide Volume 3: Analysis Procedures, Solution and Control,” New Providence, RI, 2016.

20. Luskin, L., “Report 5159-01 Dynamic Pipe Pressure Testing,” REL, Inc., Calumet, MI, 2016.

DISTRIBUTION LIST

U.S. Army ARDEC
ATTN: RDAR-EIK
RDAR-MEA-A, C. Florio
L. Reinhardt
S. Groeschler
J. Cordes
R. Lee
RDAR-WSW-F, A. Foltz
Picatinny Arsenal, NJ 07806-5000

Defense Technical Information Center (DTIC)
ATTN: Accessions Division
8725 John J. Kingman Road, Ste 0944
Fort Belvoir, VA 22060-6218

GIDEP Operations Center
P.O. Box 8000
Corona, CA 91718-8000
gidep@gidep.org

REVIEW AND APPROVAL OF ARDEC REPORTS

THIS IS A:

[X] **TECHNICAL REPORT** [ ] **SPECIAL REPORT**

[ ] **MEMORANDUM REPORT** [ ] **ARMAMENT GRADUATE SCHOOL REPORT**

FUNDING SOURCE ARDEC Institute for Special Warfare
[e.g., TEX3; 6.1 (ILIR, FTAS); 6.2; 6.3; PM funded EMD; PM funded Production/ESIP; Other (please identify)]

Development of a method for modeling the response of a liquid-filled deformable pipe to an impact load	ARDEC Institute for Special Warfare
Title	Project
Catherine S. Florio	
Author/Project Engineer	Report number/Date received (to be completed by LCSD)
(973)724-6267 / 94, Second Floor	RDAR-MEA-A
Extension / Building	Author's Office Symbol

PART 1. **Must be signed before the report can be edited.**

a. The draft copy of this report has been reviewed for technical accuracy and is approved for editing.

b. Use Distribution Statement A[X], B[ ], C[ ], D[ ], E[ ], or F[ ] for the reason checked on the continuation of this form. Reason: _____

1. If Statement A is selected, the report will be released to the National Technical Information Service (NTIS) for sale to the general public. Only unclassified reports whose distribution is not limited or controlled in any way are released to NTIS.

2. If Statement B, C, D, E, or F is selected, the report will be released to the Defense Technical Information Center (DTIC) which will limit distribution according to the conditions indicated in the statement.

c. The distribution list for this report has been reviewed for accuracy and completeness.

Aisha Haynes 6/30/17
Division Chief (Date)

PART 2. To be signed either when draft report is submitted or after review of reproduction copy.

This report is approved for publication.

Edward Bauer 9/24/18
Division Chief (Date)

RDAR-CIS (Date)

LCSD 49 (1 Sept 16)
Supersedes SMCAR Form 49, 20 Dec 06